

MIT Open Access Articles

*Automation of Challenging Spatial-Temporal
Biomedical Observations With the Adaptive
Scanning Optical Microscope (ASOM)*

The MIT Faculty has made this article openly available. **Please share** how this access benefits you. Your story matters.

Citation: Potsaid, B., F.P. Finger, and J.T. Wen. "Automation of Challenging Spatial-Temporal Biomedical Observations With the Adaptive Scanning Optical Microscope (ASOM)." *Automation Science and Engineering*, IEEE Transactions on 6.3 (2009): 525-535. © Copyright 2009 IEEE

As Published: <http://dx.doi.org/10.1109/tase.2009.2021358>

Publisher: Institute of Electrical and Electronics Engineers

Persistent URL: <http://hdl.handle.net/1721.1/60239>

Version: Final published version: final published article, as it appeared in a journal, conference proceedings, or other formally published context

Terms of Use: Article is made available in accordance with the publisher's policy and may be subject to US copyright law. Please refer to the publisher's site for terms of use.



Automation of Challenging Spatial-Temporal Biomedical Observations With the Adaptive Scanning Optical Microscope (ASOM)

Benjamin Potsaid, *Member, IEEE*, Fern P. Finger, and John T. Wen, *Fellow, IEEE*

Abstract—Biological studies, drug discovery, and medical diagnostics benefit greatly from automated microscope platforms that can outperform even the most skilled human operators in certain tasks. However, the small field-of-view of a traditional microscope operating at high resolution poses a significant challenge in practice. The common approach of using a moving stage suffers from relatively low dynamic bandwidth and agitation to the specimen. This paper describes an automated microscope station based on the novel Adaptive Scanning Optical Microscope (ASOM), which combines a high-speed post-objective scanning mirror, a custom design scanner lens, and a microelectromechanical systems (MEMS) deformable mirror to achieve a greatly expanded field-of-view. After describing the layout and operating principle of the ASOM imaging subsystem, we present a system architecture for an automated microscope system suitable for the ASOM's unique wide field and high-speed imaging capabilities. We then describe a low-cost experimental prototype of the ASOM that demonstrates all critical optical characteristics of the instrument, including the calibration of the MEMS deformable mirror. Finally, we present initial biological (living nematode worms) imaging results obtained with the experimental apparatus and discuss the impact of the ASOM on biomedical imaging activities.

Note to Practitioners—From an optical system design perspective, it is particularly challenging to design and manufacture optical imaging systems that simultaneously achieve high resolution, a wide field-of-view, and a flat image field. Consequently, a cost effective and common solution is to use off-the-shelf microscope objectives for biomedical imaging applications. However, due to optical limitations and a finite number of pixels on the camera,

the field size (observable region of the specimen) is quite small at high resolution. A common solution is to use a moving stage to translate the specimen underneath the microscope. However, for high-throughput imaging or for challenging biological observations, the moving stage is limited by a relatively slow dynamic speed and agitation of the specimen or workspace. A new microscope design, called the ASOM uses a recently commercialized MEMS deformable mirror technology in a novel optical configuration to expand the field-of-view without sacrificing resolution. Described as part of a microscope imaging workstation, the ASOM has the potential to improve throughput, increase productivity, and perform challenging spatial-temporal observations in certain biological and medical applications.

Index Terms—Adaptive optics, biology, medicine, microscopy, wide field imaging.

I. INTRODUCTION

THE introduction of digital cameras, motorized stages, and image processing to optical microscopy has had a profound effect on fundamental biological research, drug discovery, and medical diagnostics. Combining automation of the imaging hardware with image processing and robotic manipulation allows for monitoring and interacting with biological samples in ways far beyond the capabilities of even the most skilled human operator. For example, such systems can capture and track events that are much too fast for human reaction times (e.g., tracking rapidly moving motile organisms [1]), large samples can be observed over a time frame of days to weeks to glimpse rare events or increase the strength of statistical arguments [2], and large numbers of samples can be automatically processed and scored as required in drug discovery efforts where only a small portion of the prospective treatments turn out to be effective.

In general, the motivation for applying automation to microscope-based workstations are related to the following issues or limitations of the optical microscope.

- There is an inherent tradeoff between the field-of-view and resolution of the imaging system. Thus, large regions of a sample can not be imaged at a high resolution with one camera exposure.
- The depth of field associated with high numerical aperture microscope objectives is quite small, which causes blurring of the sample if it is not at the optimal distance from the objective.
- Automated analysis or processing systems require that the samples themselves be stored, transported, and loaded into the microscope.

Manuscript received October 17, 2008. First published May 26, 2009; current version published July 01, 2009. This paper was recommended for publication by Associate Editor P. Fiorini and Editor D. Meldrum upon evaluation of the reviewers' comments. This work was supported in part by the National Science Foundation (NSF) Smart Lighting Engineering Research Center (EEC-0812056) and the GOALI grant CMS-0301827, and in part by the Center for Automation Technologies and Systems (CATS) under a block grant from the New York State Foundation for Science, Technology and Innovation (NYSTAR). J. T. Wen was supported in part by the NSFC Two-Bases Project (No. 60440420130), and the Outstanding Overseas Chinese Scholars Fund of Chinese Academy of Sciences (No. 2005-1-11), China. F. P. Finger was supported in part by NSF Grant IOS-0745080.

B. Potsaid was with the Center for Automation Technologies, Rensselaer Polytechnic Institute, Troy, NY 12180 USA. He is now with the Massachusetts Institute of Technology and Thorlabs, Cambridge, MA 02139 USA (e-mail: ben.potsaid@gmail.com).

F. P. Finger is with the Department of Biology and the Center for Biotechnology and Interdisciplinary Studies, Rensselaer Polytechnic Institute, Troy, NY 12180 USA (e-mail: fingef@rpi.edu).

J. T. Wen is with the Department of Electrical, Computer, and Systems Engineering and the Center for Automation Technologies and Systems, Rensselaer Polytechnic Institute, Troy, NY 12180 USA (e-mail: wenj@rpi.edu).

Color versions of one or more of the figures in this paper are available online at <http://ieeexplore.ieee.org>.

This paper comes with two supplementary downloadable multimedia mp4 format movie clips at <http://ieeexplore.ieee.org>.

Digital Object Identifier 10.1109/TASE.2009.2021358

- Samples may require precise *in vivo* manipulation or measurement as a part of the process, experiment, or observation.

Most automated microscopy systems are structured around a traditional optical microscope design. Relatively low-cost and standardized microscope objectives make this architecture attractive, but the small field-of-view at high resolution poses a significant challenge in practice. The most common solution to address this field-of-view versus resolution tradeoff is to use a moving stage to reposition the sample relative to the microscope optics. Indeed, many automated imaging systems retrofit a moving stage to a commercially available microscope to enlarge the field-of-view by constructing an image mosaic out of sequence of individual camera exposures [3]. However, as conceptually simple as this idea seems, the relatively large mass of the moving stage results in a low dynamic bandwidth (stage speed/acceleration) and the mechanical mechanism generates considerable positioning and repeatability errors. Furthermore, there is generally a direct tradeoff between the speed of the stage and the amount of positioning error in the stage motion [4]. Dual drive systems [5] combining lead screws with piezo positions stages can help with this tradeoff. The dynamic limitations of a moving stage are compounded when the stage is moving a temperature regulated chamber or large well plate and certain sensitive biological observation tasks [1] are also adversely influenced by the agitation of the specimen resulting from the moderate accelerations of the moving stage platform [6]. From an automated systems perspective, the moving stage is undesirable because the sample must be loaded and unloaded from the stage platform, increasing the probability of sample or slide mishandling. Furthermore, the loading and unloading operations do not modify or enhance the sample and it is a critical goal of efficient process implementation to eliminate nonvalued added operations from a production line [7]. Because of these dynamic limitations during scanning and the need to load and unload slides, the moving stage is often the source of a bottleneck in biological research or automated medical diagnostics process or prevents the observation of challenging spatial-temporal events altogether.

Recently, several novel approaches to expanding the field-of-view have been proposed, including a micro-array-based microscope [8] and wide field confocal MACROscope [9]. However, these approaches are useful for measuring predominately static specimens. This paper describes a recently developed wide field microscope concept, called the Adaptive Scanning Optical Microscope (ASOM) and an implementation that addresses the shortcomings of a traditional microscope/moving stage design. By utilizing a fast steering mirror combined with a deformable mirror to correct for off-axis aberrations in a novel optical design, the ASOM operates in a unique region of the performance domain and exhibits the following desirable characteristics.

- Rapid dynamic scanning to enlarge the field-of-view while maintaining resolution.
- No agitation to the specimen or sample during scanning.
- Efficient low light level imaging.
- Convenient integration into automated production systems using conveyor transports for part storage and presentation.

- Easy integration with robotic manipulators, sensors, or stimuli that facilitates high-speed operation and high positioning accuracy during sample manipulation or measurement.

The large field-of-view, relatively long working distance, rapid and flexible scanning capability, and ability to scan without moving the workspace make the ASOM particularly suitable for challenging biomedical imaging applications. With respect to throughput and dynamic imaging capabilities, the scanning mechanism provides scanning speeds on the order of 10–100 times faster than a moving stage, depending on the stage payload. Furthermore, the area scan camera in the ASOM is more efficient than line scanning camera-based system configurations in low light imaging applications because the pixels can be exposed simultaneously rather than sequentially. When multiple manipulators, microinjectors, or sensors are required, the ASOM excels by offering a uniform and high resolution over a greatly enlarged field-of-view. The moving stage does not offer such an attractive manipulation environment because either (1) the robotic manipulator must be mounted on the moving stage [10] with the consequence of increasing the stage mass and considerably slowing down the stage motion or (2) the robotic manipulator must be fixed to the machine base with the consequence of requiring the motion of the moving stage and the manipulator to be precisely coordinated, compromising speed and accuracy, or (3), the sample must be moved relative to the fixed manipulator [11], possibly agitating sensitive solutions. However, the field-of-view of the ASOM is not as large as the virtually unlimited field-of-view associated with a moving stage due to optical considerations in the design.

Previous work related to this research has focused on the underlying optical design and imaging principle of the ASOM [12]. Basic deformable mirror shape optimization and control methods have been experimentally demonstrated [13], and automatic tracking of nonrotating and fixed shape moving objects in a robotic workspace has been shown [14]. This paper shows for the first time the complete integration of the core ASOM technologies into an automated imaging platform with the capability to track multiple freely moving biological samples that are continuously changing shape and orientation. By identifying the different parts of the sample (head, tail, and midsection) and imaging each section with a single camera frame, the ASOM is able to efficiently construct high resolution images of the samples over their entire body length. These are critical first steps towards multiscale biological investigations, where observing individual cells at the same time as organs, animals, and populations of freely moving specimens will provide new insights into biological processes and effects of the environment.

Section II describes the ASOM imaging subsystem itself and presents simulated results of an example ASOM design. Section III describes how the ASOM can be integrated into an automated imaging platform and the overall system operation and architecture. Section IV describes an experimental ASOM apparatus, while Section V describes improvements to the shape optimization and real-time control of the deformable mirror. Section VI presents the first results of automated live organism imaging using the experimental system. Conclusions and future work are presented in Section VII.

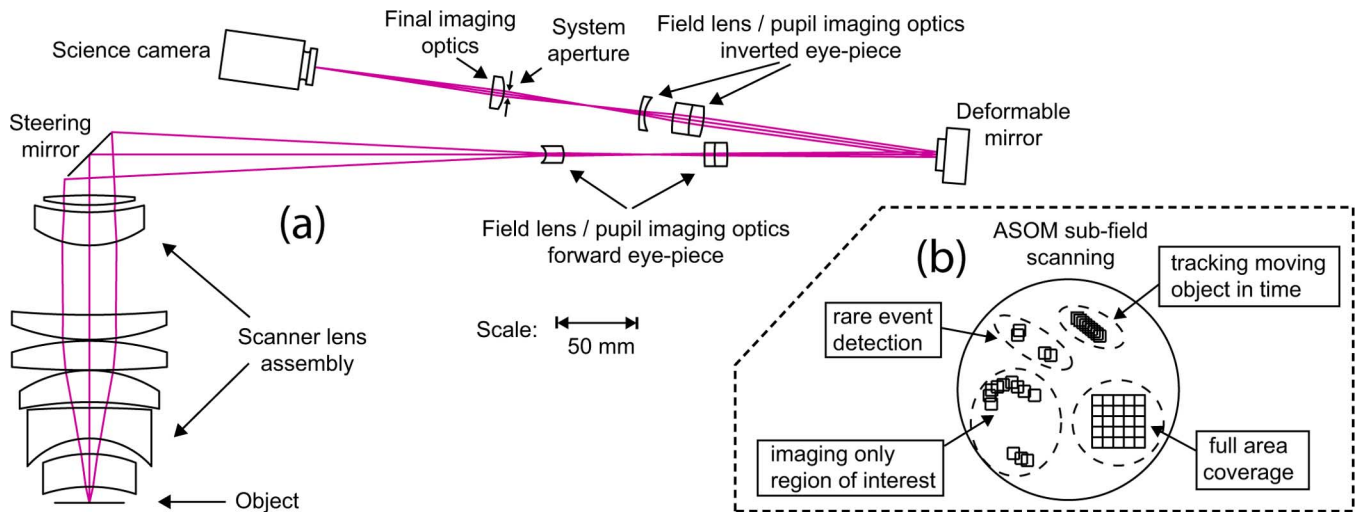


Fig. 1. (a) Preliminary ASOM design. (b) ASOM modes of operation (total field size and individual camera exposure regions are not to scale).

II. ASOM IMAGING SUBSYSTEM

At the heart of the imaging platform is the imaging subsystem itself, which consists of an ASOM. The underlying concept of the ASOM is to use a low mass steering mirror located between the scanning lens and the imaging optics to form a post-objective scanning configuration, as shown in Fig. 1(a). This allows a small sub-field-of-view to be quickly scanned throughout the workspace so that multiple disjoint or overlapping regions of the workspace can be visited and imaged in rapid succession, as illustrated in Fig. 1(b). Through image warping and mosaic construction, a large and continuous virtual image of the object or region can then be constructed from the individual image tiles. The advantages of such an arrangement are: a large effective field-of-view at high resolution, no disturbance to the sample, and high scan rate operation. However, such a system configuration also poses significant design and implementation challenges. Compared to the moving stage or moving microscope designs, there is extensive off-axis imaging (i.e., images are obtained by looking diagonally through the scan lens), which introduces image distortion in addition to contrast degrading and resolution reducing aberrations (e.g., coma, astigmatism, field curvature, etc.) [15] that have typically reduced the effectiveness of such an approach. In the ASOM, we address the off-axis aberrations by the following.

- 1) Explicitly incorporating field curvature into the design to greatly reduce the complexity of the scanning lens.
- 2) Introducing an actuated deformable mirror (DM) into the optical path to correct for the residual aberrations.
- 3) Image processing to remove image distortion.

Note that by combining dynamic components and algorithmic techniques with traditional static optical elements, the lens count in the scanner lens is greatly reduced compared to a comparable static optics only design. This results in a potential savings in manufacturing and assembly costs (lithographic projection lenses can cost in the millions of dollars [16]), making the ASOM accessible for research and production activities.

Fig. 2 shows how the angle of the steering mirror selects the location of the field-of-view within the workspace (note that a

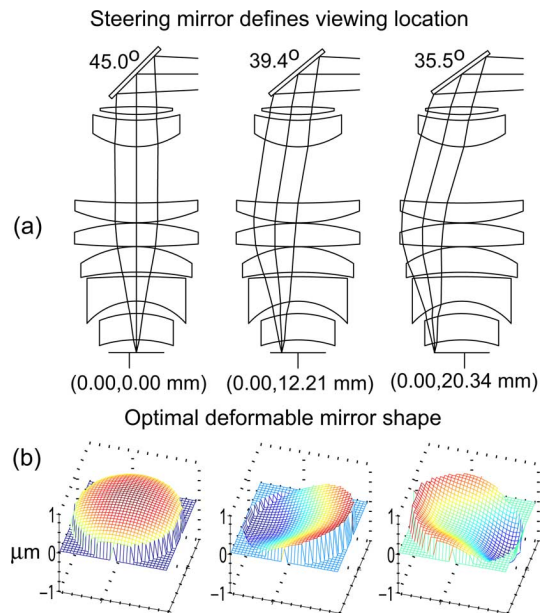


Fig. 2. (a) ASOM scanning mechanism. (b) Optimal deformable mirror shapes.

$k \times k$ pixel image is acquired at each field location rather than a single point as in confocal microscopy). A specific deformable mirror shape corrects for the aberrations unique to each field position to obtain diffraction limited performance. Without the deformable mirror, images obtained at these field positions would be blurred with such a simple scanner lens design. In practice, the deformable mirror is calibrated once during the initial construction. Then during operation, a lookup table with interpolation is used to shape the deformable mirror for each field position. Recent advances in MEMS deformable mirrors have reduced the price of this technology, making adaptive optics more affordable for research and productization [17]. Table I lists performance specifications for the simulated ASOM shown in Fig. 1(a), the experimental ASOM that was constructed, and the greatly enlarged field-of-view for the ASOM is compared to existing microscope technologies in Fig. 3. The field sizes for the

TABLE I
ASOM PERFORMANCE SPECIFICATIONS

Specification	Simulated ASOM	Experimental Prototype
Effective field of view diameter	40 mm	5 mm
Total observable field area	1257 mm ²	20 mm ²
Numerical aperture	0.21	0.1
Working distance	7 mm	10.3 mm
Operating wavelength	510 nm	510 nm
Resolution	1.5 μm	3.1 μm
Magnification	15.2	6.5
Depth of Field	13 μm	56 μm
Camera pixel count	512 × 512	768 × 475
Camera pixel size	10 × 10 μm	8.4 × 9.8 μm

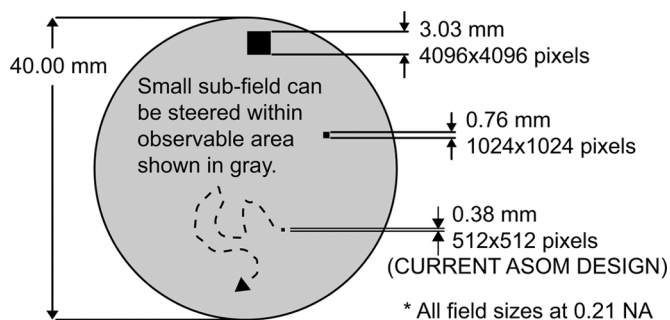


Fig. 3. Field size comparison of ASOM to standard microscopes.

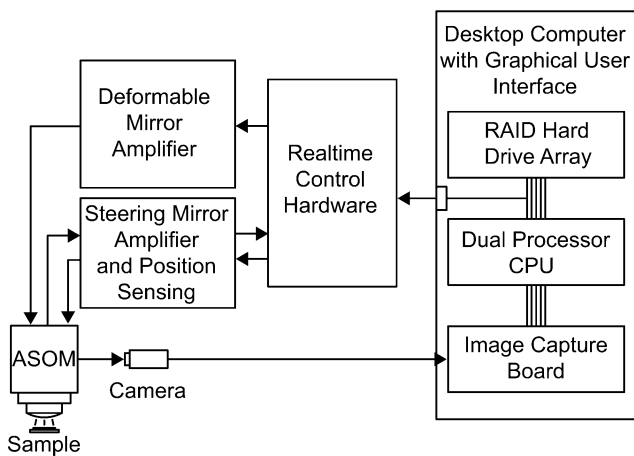


Fig. 4. System architecture.

fixed microscope designs assume perfect imaging from an optical perspective with the upper bound defined by Nyquist sampling to avoid aliasing. Thus, the number of camera pixels alone determine the maximum achievable field size at this resolution. For a more thorough discussion of the ASOM theory of operation, please see a previously published simulation-based paper [12].

III. SYSTEM ARCHITECTURE

The overall architecture for the imaging platform we are developing is shown in Fig. 4. Light from the specimen is collected by the ASOM imaging subsystem and projected onto the sensor of a digital camera. The camera digitizes the image and transfers the data to a frame grabber residing in a computer with a multi-core processor. The image processing routines locate objects of

interest within the image or determine regions of interest. Coordinates for the next scan pattern can then be determined from the processed data and the image data saved on the computer's hard drive. A redundant array of independent disks (RAIDs) is required to maintain the high data transfer rates as continuous data rates for single hard drives are too slow for certain high-speed cameras. The coordinates of the regions of interest are then transmitted to the real-time control computer, where the motion path planner generates a new trajectory for the steering mirror. The real-time control computer also controls the steering mirror with a closed loop controller and voltage signals are generated to drive the deformable mirror amplifier.

When tracking rapidly moving objects, a moving stage-based approach is typically limited to observing only one object [1]. Thus, image exposure, data transfer, processing, and motion must be performed *serially* in time as each step depends on the previous step having been completed. The rapid dynamic performance of the ASOM allows multiple rapidly moving objects to be tracked. A significant consequence of tracking more than one object is that image processing can be performed in *parallel* to the data transfer, motion, and image processing events of other objects. This is demonstrated in Fig. 5, which shows a possible operational timing diagram of the imaging platform. In this diagram, it is assumed that the system is tracking the motion of three objects and that the frame rate of the camera is constant at 100 frames/s. Events associated with each of the three objects are noted with a circled "1," "2," or "3." First, the deformable mirror is commanded to produce the required shape to compensate for the off-axis aberrations and the steering mirror is commanded to the angle required to steer the field-of-view into the desired position. After settling of the mirrors, the camera exposure takes place and the data transfer from the camera to the image processing hardware begins. Once transferred, the image is processed and key features are extracted to determine new coordinates for the field-of-view associated with that object. However, after acquiring images from each object, notice that the deformable mirror and steering mirror are free to move into the next position *at the same time* as the data transfer and image processing are taking place associated with the previous object. In fact, the advantage of parallelizing the image processing operations increases with the number of objects being tracked until the data transfer rate or mirror dynamics become the limiting factor. Note that full multiprocessor parallel computing has not yet been implemented in the experimental apparatus described next, however, processing images from previous events at the same time as mirror movements has been implemented for improved performance.

IV. OVERVIEW OF EXPERIMENTAL APPARATUS

The discussion and performance specifications for the ASOM presented in Section II are based on high fidelity simulated results of a system that uses a 100 actuator deformable mirror and custom fabricated optics. The purpose of this experimental ASOM apparatus was to demonstrate all essential optical aspects of the ASOM design. For budgetary reasons (approximately \$13 K for hardware) and to shorten development time, a

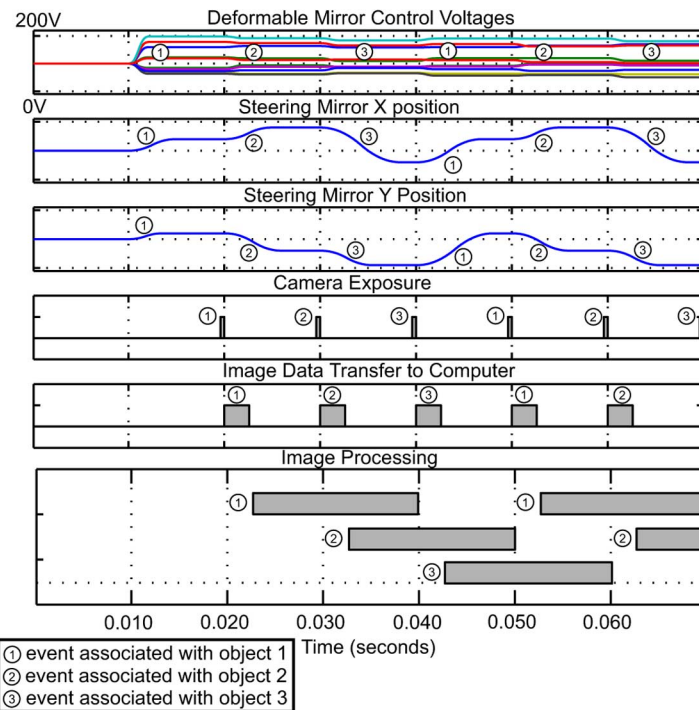


Fig. 5. Timing diagram showing the coordination of the different ASOM components and processes during the tracking of multiple moving objects or events using parallel processing.

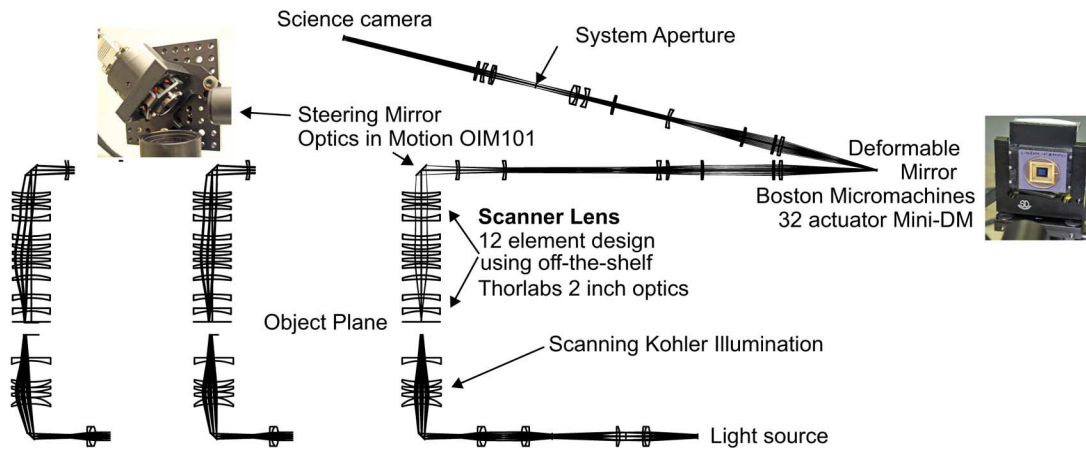


Fig. 6. ASOM experimental layout.

lower cost 32 actuator deformable mirror and off-the-shelf optics were used in this first prototype. However, most stock lenses are designed to be used in a particular manner (e.g., with infinite conjugates) for generic applications and are offered in a coarse range of focal distances, lens diameters, and glass selections. Considering the atypical imaging characteristics of the scanner lens, the experimental ASOM design using off-the-self optics only is far from optimal, and as such, exhibits a noticeably high lens count to achieve 0.1 NA over a nominal 20 mm field size. However, even with the use of off-the-shelf optics only, this experimental apparatus has been carefully designed to demonstrate all of the *critical optical characteristics* that define the ASOM, including the curved field optical scanning approach and wavefront correcting optics using a deformable mirror. Future experimental work will utilize custom manufactured optics

to fully realize the potential of the ASOM concept to achieve higher numerical aperture and/or a larger workspace to meet the requirements of different applications.

Fig. 6 shows the optical layout of the experimental setup and Fig. 7 shows a picture of the prototype ASOM. This prototype utilizes a galvanometer-based scanning Kohler illumination system such that only the region being imaged is illuminated by the transmitted light, reducing phototoxicity effects on living specimens. Since the current design is very sensitive to chromatic aberration, a 510 nm wavelength bandpass filter is included in the illumination stage to eliminate much of the light spectra below 505 nm and above 515 nm. Light transmits through the sample and is then collected by the telecentric 12 element scanner lens assembly. An electromagnetically actuated fast steering mirror (FSM) with a flexure suspension (Optics in

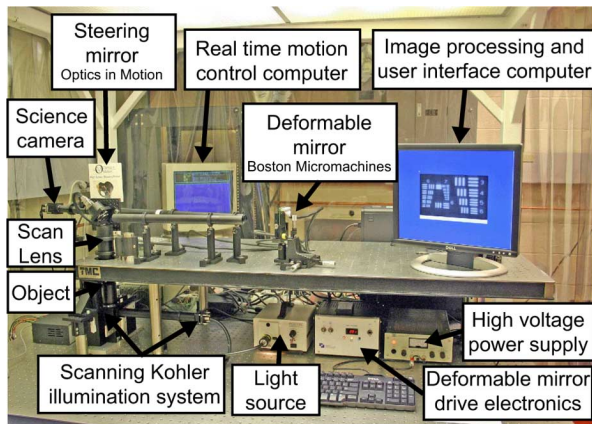


Fig. 7. ASOM prototype built with off-the-shelf optics.

Motion OIM101) has two degrees of freedom to steer the sub-field-of-view within the workspace. Optics project the light onto the MEMS deformable mirror (Boston Micromachines Mini-DM). By precisely controlling the shape of the reflective surface of the mirror to be opposite the shape of the wavefront error (but at half the amplitude), the deformable mirror can correct for the wavefront aberrations to within the diffraction limit. This mirror has 32 electrostatic actuators with $400\ \mu\text{m}$ actuator spacing, a $2.5\ \mu\text{m}$ actuator stroke, and a $2.0\ \text{mm}$ diameter actively controlled area. The $2.5\ \mu\text{m}$ stroke is capable of correcting for up to several waves of aberration, which allows for high image quality even for the off-axis field positions and enables the greatly expanded field-of-view in the ASOM. Additional optics project the final image onto the CCD camera (Pulnix TM200). A host computer acquires (MATROX Meteor II frame grabber) and processes the images. A second computer is dedicated for real time control running MATLAB xPC Target and implements the digital control/trajectory generation algorithms for the FSM and generates galvanometer position commands for the scanning illumination system. Note that parallel processing has not yet been implemented on this testbed, but is currently under development along with integration of a high-speed camera to replace the existing Pulnix TM200 running at 30 frames/s.

V. DEFORMABLE MIRROR SHAPE OPTIMIZATION

The simulated ASOM design shown in Fig. 1(a) was designed around the μDM100 deformable mirror from Boston Micromachines (Watertown, MA) with 140 electrostatic actuators, a $3.3\ \text{mm}$ round aperture, a $2\ \mu\text{m}$ stroke, and a $1\ \text{kHz}$ update rate [18]. The actuators are arranged in a 12×12 actuator grid pattern, minus the four corner actuators. Similarly, the experimental ASOM shown in Fig. 7 uses the lower cost version of this mirror with only 32 actuators in a 6×6 actuator grid pattern, minus the four corner actuators. Differing than most other MEMS membrane deformable mirror technologies commercially available today, a unique characteristic of the Boston Micromachines deformable mirror technology is the inclusion of a third layer in the design, as shown in Fig. 8(a). This third layer is a thin silicon beam that is doubly cantilevered at both ends and suspended over an electrostatic actuator pad located

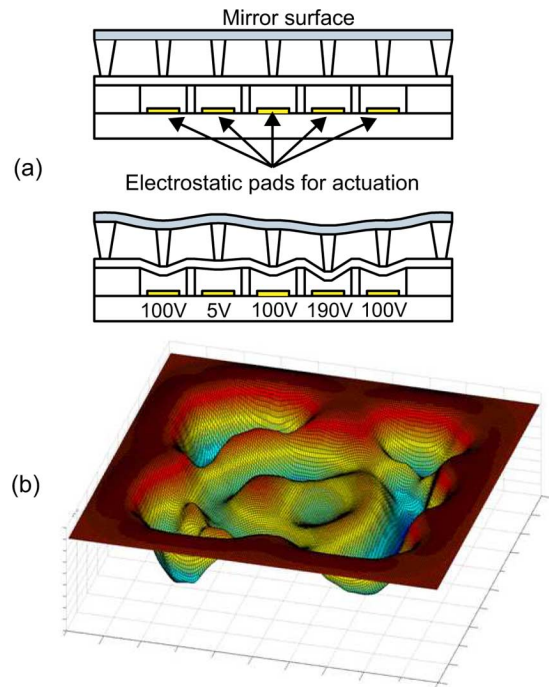


Fig. 8. (a) MEMS deformable mirror architecture. (b) Example deformable mirror shape profile.

underneath the actuator's bottom surface. Each actuator is attached to the deformable mirror's continuous facesheet by a thin post. By holding the actuator beam at a constant voltage and charging the pad below, an attractive electrostatic force pulls down on the actuator beam. Conversely, if the voltage is removed from the actuator pad, the stiffness of the doubly cantilevered beam acts as a restoring force which can push upwards on the facesheet surface. A typical usage scenario of this type of deformable mirror is to bias all of the actuators to a voltage that deflects the mirror to approximately half of the total stroke capability. In this way, reducing the voltage to an actuator results in a localized positive surface deflection and increasing the voltage to an actuator results in a localized negative surface deflection. A wide range of surface shapes can be generated in this manner [19], including the example profile shown in Fig. 8 obtained from a high fidelity deformable mirror simulation.

Allowing for significant aberration in the scanner lens and correcting for the aberration with a MEMS deformable mirror is a key idea in the ASOM to achieve a wide field-of-view at a relatively low-cost for the static optical elements (lenses). The specific shape and size of the aberration depends on the field position, but it is important that the rate of change in the aberration between field positions be sufficiently small as to allow a diffraction limited image over one instantaneous field-of-view (image exposure). For any given field position, however, the aberrations are static as the glass causing the aberration is stationary, and because the electrostatic MEMS deformable mirrors do not exhibit hysteresis [19], an open loop strategy can be utilized for the deformable mirror control to achieve high-speeds during operation. First, the appropriate deformable mirror shape must be determined through a calibration procedure and the results stored. Then, during operation, the

actuator voltages to the deformable mirror, V are reconstructed as a function of the current field position as determined by the steering mirror angles, θ_x and θ_y

$$V = f(\theta_x, \theta_y). \quad (1)$$

In simulation, perfect knowledge of the wavefront shape is readily available and it is straightforward to numerically determine the required mirror shape to correct for the specific aberrations associated with each field position. However, in practice, manufacturing tolerances and assembly errors introduce unmodeled aberrations into the optical system. Furthermore, internal residual stresses combined with manufacturing variations result in surface bowing in the MEMS deformable mirror, as well as actuator performance variation [20]. Thus, experimental use of the deformable mirror requires a method for the *in situ* shape optimization of the deformable mirror surface. If we consider the inputs of the optimization to be the deformable mirror actuator voltages, V , and Q to be some metric of the image quality or residual aberration, then the experimental deformable mirror shape optimization requires:

- a metric to represent the image quality or residual aberration, $Q(V)$;
- an optimization algorithm to minimize $Q(V)$.

The metric $Q(V)$ is, in general, a nonlinear function of the actuator voltages, V and $Q(V)$ is defined to decrease with improving image quality. The resulting optimization problem is also subject to upper and lower bounds on the actuator voltages. Methods and approaches for optimization constitute an active field of research on its own and there are many possible image quality metrics and optimization methods that can potentially be combined for the ASOM deformable mirror shape optimization.

In practice, the wavefront cannot be measured directly, but must be inferred from a related measurement of light intensity. Often a wavefront sensor (e.g., Shack Hartmann [21]) is used. Other common methods include interferometry or algorithmic techniques such as phase diversity using two or more cameras at different focal planes [22]. For the ASOM, it is advantageous from a cost and complexity perspective to use a technique based on the image quality alone, not requiring any additional hardware or layout reconfiguration. Various metrics have been proposed for automatically assessing the quality of an image, including image entropy [23] and image sharpness via high-pass filtering [24].

The image quality metric used for the optimization in this research is based on image sharpness as defined by Muller and Buffington [25], where the quality of the image is sharpest when the metric, Q , is minimized. Given an $i \times j$ matrix of intensity values to represent the image, I , the specific image quality metric, Q is defined as

$$Q = - \sum_i \sum_j I_{i,j}^2. \quad (2)$$

Optimization of the image quality metric was performed with a steepest descent algorithm. First, a linear approximation to the gradient was obtained by finite different perturbations to the individual actuator voltages to obtain $\nabla Q(V) = \partial Q / \partial V$. Next, a line search was performed along the steepest descent direction

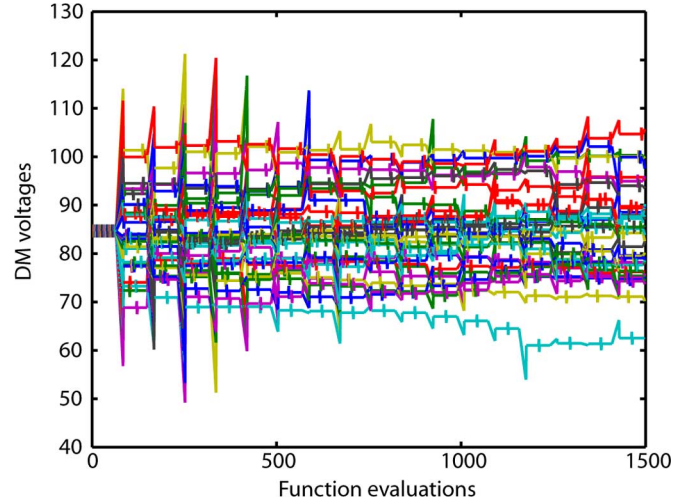


Fig. 9. Deformable mirror actuator voltages versus optimization iterations.

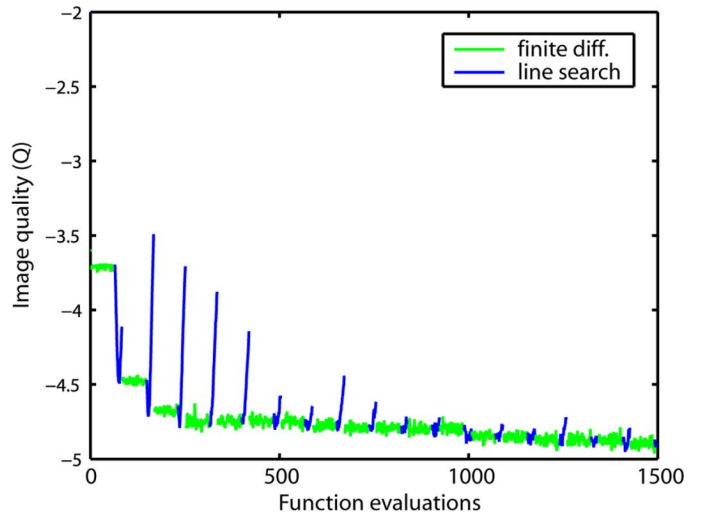


Fig. 10. Image quality versus optimization iterations.

$(-\nabla Q(V))$ to obtain an optimal step size, with the voltages updated accordingly. Since the gradient is only an approximation to the true nonlinear system, the solution at this point is sub-optimal. Thus, the process of finite different perturbations and line searches is repeated until convergence is achieved. Fig. 9 shows the evolution of the 32 deformable mirror actuator voltages for each optimization iteration and Fig. 10 shows the associated image quality metric (the relatively flat regions represent finite difference perturbations and the curved regions indicate the line search portion of the optimization algorithm). In these plots, a single function evaluation indicates a single deformable mirror update, or equivalently, a camera exposure event. All actuators start at 85 volts, which is slightly less than half the voltage supply. Based on the image of the USAF 1951 calibration target shown in Fig. 11 before and after optimization, it is clear that the image quality improves as the shape of the deformable mirror is optimized. The smallest bar pattern can be clearly resolved in the optimized image and represents a resolution of about 4 microns. The theoretical resolution of the low-cost ASOM apparatus is about 3.1 microns (0.1 NA at

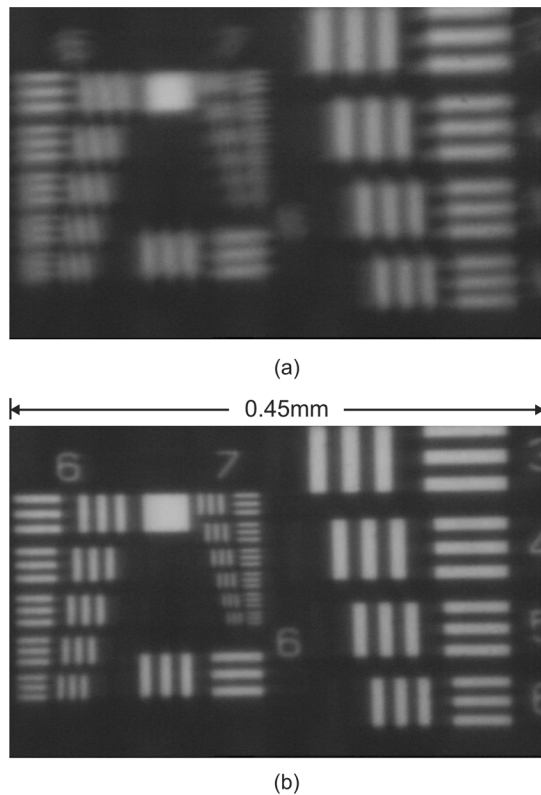


Fig. 11. Image of USAF 1951 calibration target: (a) before and (b) after optimization.

$\lambda = 510$ nm), which indicates that the aberrations have been reduced to being close to, or exceeding the diffraction limit.

The optimal set of voltages for the deformable mirror in the ASOM must be determined in an offline training process before operation. Then, during operation, the deformable mirror voltages can simply be recalled from a set of previously stored values. Since it is not practical to optimize for every possible field position, we optimize a grid sampling of points over the entire observable field-of-view and use interpolation of the deformable mirror actuator voltages for field positions that lie between calibration points. Due to the constraint of using off-the-shelf optics in the low-cost ASOM prototype, the magnitude and variation of the aberrations introduced by the scanner lens are relatively small, but significant enough to noticeably degrade the image quality. We are, therefore, able to use a 5×5 grid of calibrated points to cover the entire observable field-of-view (approximately $5.0 \text{ mm} \times 3.5 \text{ mm}$ in this implementation). During ASOM operation, bilinear interpolation is used to estimate the optimal set of actuator voltages in between the calibrated data points that include the current operating position. More information about deformable mirror calibration and interpolation during runtime can be found in a related paper [13].

VI. IMAGING LIVING *CAENORHABDITIS ELEGANS* NEMATODE WORMS

The nematode worm, *Caenorhabditis elegans* (*C. elegans*), exhibits a remarkable balance between sophistication for research in developmental and neurobiology, as well as manageability with respect to complexity. An adult *C. elegans* hermaphrodite contains precisely 959 somatic nuclei, of which

exactly 302 are neuronal. Furthermore, the full cell lineage is known [26], [27], and the synaptic connectivity of the nervous system has been completely mapped by serial section electron microscopy [28]. One of the simplest and best documented animals having demonstrated multiple modes of learning [29], possessing many of the essential attributes of more complex animals with respect to physiology [30], and exhibiting a translucent body which is easily imaged with a microscope, *C. elegans* is a near ideal test specimen and model system for many investigatory neural and biological studies.

To the best of the authors' knowledge, all attempts to image live and motile *C. elegans* have been performed *either* on multiple worms at low resolution *or* a single worm at high resolution (or possibly several touching or nearly touching worms in a single field-of-view). For imaging a large population of worms, a low magnification objective [31] is often used to circumvent the problem of worms migrating outside of the field-of-view. However, at low magnification, it is difficult to accurately identify many phenotypes [32] and to resolve details such as individual cells and organs. Switching to a high-resolution objective allows imaging the worms in greater detail, but introduces the challenge of the worm migrating outside of the small field-of-view. For high-resolution imaging of the worms, a moving stage is often used with the microscope and controlled by real-time image processing routines to keep the worm centered in the field-of-view [33]. Other work [34] uses both high and low magnification microscope objectives simultaneously for monitoring gross worm behaviors and neural activities, respectively. Alternatively, the worm can be immobilized, either with adhesive fixing the tail or by partial paralyzation [35]. However such approaches interfere with the worms' natural behavior and stress the animals. The unique imaging capabilities of the ASOM offer an opportunity to address some of these limitations of a conventional microscope approach.

As described in Section II, the ASOM can achieve rapid dynamic imaging of multiple moving objects over relatively large spatial distances. This capability opens the possibility of advancing towards true multiscale biological investigations, e.g., the simultaneous imaging of individual cells, organs, and animals within a population of freely moving, interacting, and unrestrained organisms. As a first step towards this goal, Fig. 12 shows how the ASOM can automatically track and image a freely moving *C. elegans* worm at high resolution. Differing significantly from previous worm imaging approaches, high resolution is maintained in this demonstration by covering the worm with three separate camera exposures as can most clearly be seen in Frame 1320 of Fig. 12. A real-time worm tracking algorithm identifies the locations of the head, tail, and midsection between frames and automatically directs the ASOM to image these regions in rapid succession.¹ It is in this manner that wide field imaging is achieved without compromising resolution. Indeed, the effective pixel count of the combined image mosaic can be much larger than a single camera will allow. However, the requirements of the tracking algorithm differ than previous methods in that only a portion of the worm is visible within

¹This paper comes with supplementary downloadable material provided by the authors. Includes two multimedia mp4 format movie clips, which show video footage associated with Figs. 12 and 13. This material is 3.8 MB in size.

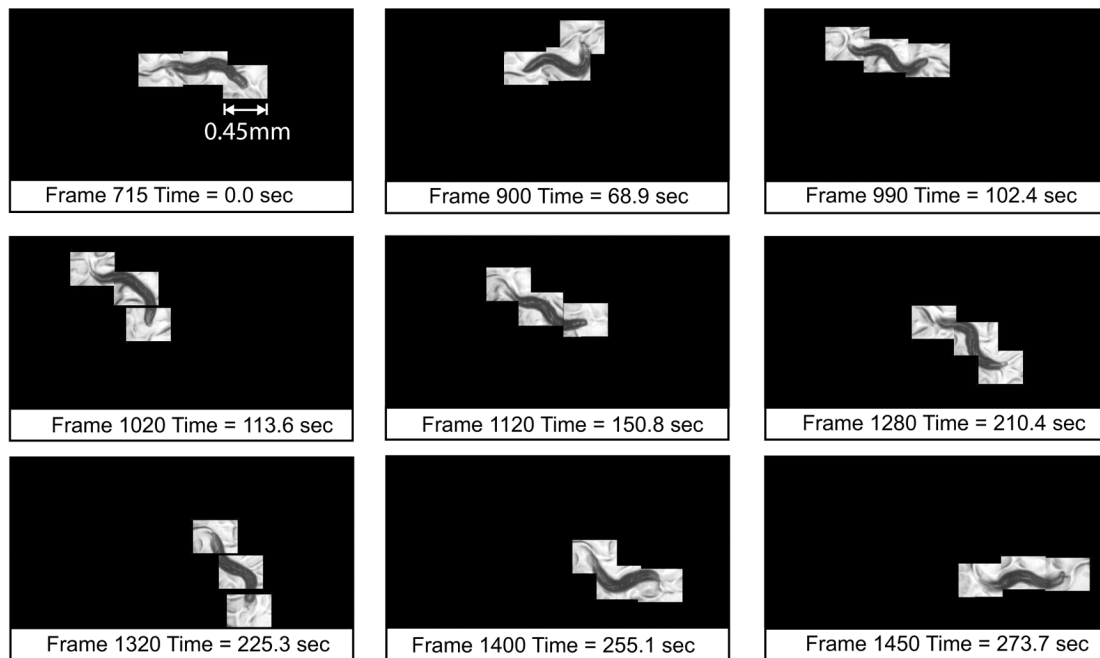


Fig. 12. Imaging multiple living *C. elegans* worms with the prototype ASOM. Three individual camera exposures are used to image each worm to achieve high-resolution imaging over a large field-of-view. The ASOM dynamically adjusts the scan pattern to place the image tiles on the head, tail, and midsection.

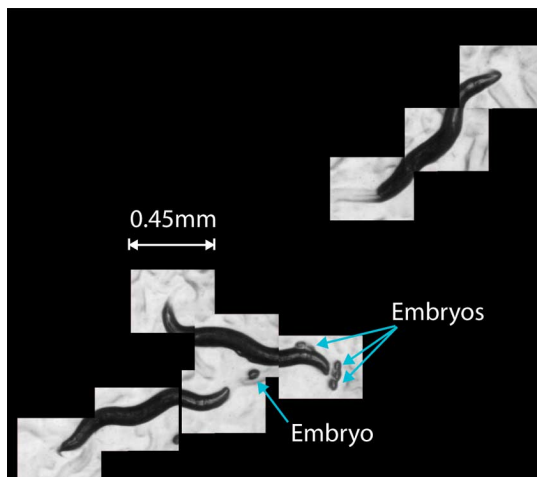


Fig. 13. Simultaneous tracking of three worms, each with three image tiles per worm using the prototype ASOM.

each single camera image rather than the entire worm. To be described in more detail in a future publication, the tracking algorithm used in this research was inspired by knowledge of the worm's locomotion capabilities and is based on minimizing metric functions associated with head and tail motion (obtained by carefully shifted and aligned image subtraction) and information associated with the worm's previous configuration and orientation. As such, the tracking algorithm works well at rejecting background objects (such as the worm eggs seen in Fig. 13), but, in its current implementation, is sometimes confused when multiple worms occupy the same space. Note that more sophisticated worm tracking and segmentation algorithms may be better able to track touching and overlapping worms. However, such algorithms tend to be computationally unsuitable for real-time

implementation as required here. They are usually used for off-line postprocessing of previously recorded results [32]. The current algorithm runs on the 3 GHz Pentium D computer in less than 0.3 ms on average per worm, which is well suited to the dynamic capabilities of the ASOM demonstration apparatus which currently has rest-to-rest mirror settling times on the order of 2.5 ms–6.0 ms [13] between field positions. Fig. 13 shows how the basic algorithm, which was implemented as a C++ object with an instance associated with each worm, can be extended to image multiple worms nearly simultaneously. During the time period of steering mirror movements associated with the first worm, the worm tracking algorithm can process the images associated with the second worm, demonstrating the potential time sharing advantages of a parallel processing approach, as illustrated in Fig. 5.

The video footage shown in Figs. 12 and 13 was obtained from *C. elegans* on a bacterial lawn supported by Nematode Growth Medium agar in a petri dish. In a different imaging experiment, Fig. 14 shows a five tile image mosaic of several worms and larvae mounted on a 5% agarose pad on a slide. These animals were alive and moving, but their motion was inhibited by being sandwiched between the coverglass and the agarose. Obtained at the same resolution as the freely moving footage shown in Figs. 12 and 13, Fig. 14 shows that imaging through the microscope slide results in greater clarity of the internal worm structure as the worm is somewhat flattened, creating a thinner specimen to image. Additionally, the light is brighter, not having passed through a thick agar medium. Future work will combine the automatic tracking of multiple freely moving worms with epi-illuminated fluorescent imaging of particular cells or organs within their bodies. Note that the basic principle of fluorescent imaging with the ASOM have been demonstrated in a previous paper [36], which also

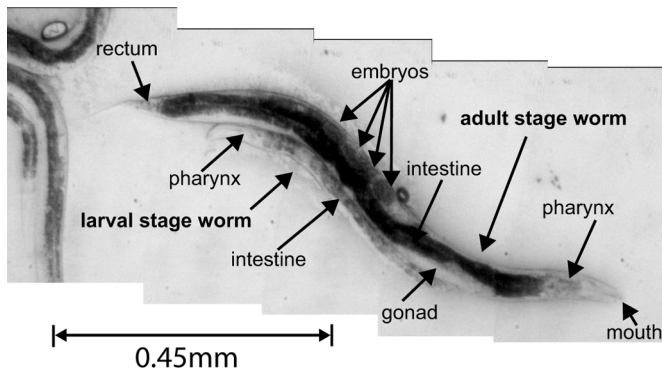


Fig. 14. Imaging a single worm on a microscope slide with five image tiles.

discusses in greater detail the advantages of low light dosage illumination inherent in the ASOM design.

VII. CONCLUSION

We present an automated microscope station based on the Adaptive Scanning Optical Microscope (ASOM), which has certain advantages over the existing moving stage approach with respect to dynamic performance, throughput, and no agitating to the specimen during scanning. These features make the microscope particularly suitable for challenging spatial-temporal biomedical observations. The performance advantage of the ASOM is achieved by combining a high-speed post-objective scanning mirror with a custom design scanner lens and a deformable mirror in a novel microscope configuration. During high-speed operation, the microscope system will generate considerable amounts of data which requires careful consideration of the system architecture. We propose that high bandwidth data busses, multiple processors, and parallelization of the image processing and motion tasks are thus required. A proof of concept experimental apparatus has been constructed and demonstrates all of the critical optical aspects of the ASOM using off-the-shelf optics, a 32 actuator MEMS deformable mirror, and a high-speed steering mirror. We have used this experimental hardware to performed initial demonstrations, imaging multiple freely moving *C. elegans* nematode worms at high resolution over a large field-of-view.

The ASOM as simulated in this paper images a field approximately two orders of magnitude larger in area (40 mm diameter at 0.21 NA) than a traditional microscope design, which is well suited for many practical biological applications. Limitations in the scan lens related to the angles of incidence of the light rays on the glass surfaces create an upper bound on the achievable field size. For applications requiring even larger fields, mating the ASOM with a moving stage could offer many of the benefits of the ASOM, while alleviating the agitation and speed disadvantages of the moving stage by coordinating the motion trajectories of the two scanning components. The low-cost ASOM prototype presented in this paper images over a narrow wavelength band that is centered at 510 nm with an approximate 10 nm full width half max (FWHM), a limitation originating from the use of off-the-shelf optics only. This is appropriate for general biological imaging as green light is relatively safe for the living organisms, but does limit the light collecting capability

and sensitivity of the instrument. Designs using custom ground optics and the appropriate selection of glass types will allow the width of the imaging band to be improved and tailored to a specific application. Defining the ultimate limits on the achievable bandwidth is a topic of ongoing research and it is unclear at this time how large the bandwidth can be made because of the difficulty in designing chromatically corrected systems with an aperture external to any glass symmetry. However, even with a narrow bandwidth, the ASOM is useful for many biological and industrial applications.

We are currently integrating a high-speed camera and multi-processor computer into the ASOM imaging system and will soon begin a series of biological studies with the apparatus. Experiences learned during this first round of studies will help us design the next-generation prototype that will include custom manufactured optical elements, a larger diameter high-speed steering mirror, and 100 actuator MEMS deformable mirror to realize the full potential of the instrument. Ultimately, the ASOM will benefit high-throughput medical research and diagnostics, as well as enable certain challenging spatial-temporal biological investigations. However, the ASOM also has applications outside of a biomedical context. Many of the same advantages of the ASOM are also beneficial for industrial manufacturing, microsystems research, and inspection. Since the development of this initial ASOM prototype, Thorlabs Inc., an expert optics and instrumentation company, has licensed the ASOM technology and is bringing an ASOM product to market. More details about the process of technology transfer, commercialization, and productization can be found in a related paper [37].

ACKNOWLEDGMENT

The authors would like to thank C. A. Morton and L. I. Rivera for their contributions to the worm imaging experiments.

REFERENCES

- [1] N. Ogawa, H. Oku, K. Hashimoto, and M. Ishakawa, "Microrobotic visual control of motile cells using high-speed tracking system," *IEEE Trans. Robotics*, pp. 1–9, 2005.
- [2] F. Ianzini, L. Bresnahan, L. Wang, K. Anderson, and M. Mackey, "The large scale digital cell analysis system and its use in the quantitative analysis of cell populations," in *Proc. 2nd IEEE-EMB Conf. Microtechnol. Med. Biol.*, 2002, pp. 469–475.
- [3] S. K. Chow, H. Hakozaki, D. L. Price, N. A. B. Maclean, T. J. Deerinck, J. C. Bouwer, M. E. Martone, S. T. Peltier, and M. H. Ellisman, "Automated microscopy system for mosaic acquisition and processing," *J. Microscopy*, vol. 222, pp. 76–84, May 2006.
- [4] J. Zemek, C. Monks, and B. Freiberg, "Discovery through automation," *Biophotonics Int.*, vol. 10, no. 4, pp. 54–57, May 2003.
- [5] X. Xie and R. Du, *Research on Key Techniques of Nanometer Scale Macro-Micro Dual-Drive Precision Positioning*, L. Yang, Y. Chen, E.-B. Kley, and R. Li, Eds. Bellingham, WA: SPIE, 2007, vol. 6722, 1, p. 67220F. [Online]. Available: <http://link.aip.org/link/?PSI/6722/67220F/1>
- [6] M. Oheim, "High-throughput microscopy must reinvent the microscope rather than speed up its functions," *British J. Pharmacology*, vol. 152, no. 1, pp. 1–4, 2007.
- [7] M. P. Groover, *Automation, Production Systems, and Computer-Integrated Manufacturing*. Englewood, NJ: Prentice-Hall, 2001.
- [8] R. S. Weinstein *et al.*, "An array microscope for ultrarapid virtual slide processing and telepathology. design, fabrication, and validation study," *Human Pathology*, vol. 35, no. 11, pp. 1303–1314, 2004.
- [9] P. Constantinou, T. Nicklee, D. Hedley, S. Damaskinos, and B. Wilson, "A high-resolution microscope with differential phase contrast, transmitted light, confocal fluorescence, and hyperspectral capabilities for large-area tissue imaging," *IEEE J. Sel. Topics Quantum Electron.*, vol. 11, no. 4, pp. 766–777, Jul.–Aug. 2005.

- [10] K. Inoue, T. Arai, T. Tanikawa, and K. Ohba, "Dexterous micromanipulation supporting cell and tissue engineering," in *Proc. 2005 IEEE Int. Symp. Micro-NanoMechatronics and Human Sci.*, Nov. 7–9, 2005, pp. 197–202.
- [11] H. Takamatsu, S. Uchida, and T. Matsuda, "A method for in-situ targeting and harvesting of cultured cells under a microscope," in *2006 Int. Symp. Micro-NanoMechatronics and Human Sci.*, Nov. 5–8, 2006, pp. 1–4.
- [12] B. Potsaid, Y. Bellouard, and J. Wen, "Adaptive scanning optical microscope (ASOM): A multidisciplinary optical microscope design for large field of view and high resolution imaging," *Opt. Express* no. 17, pp. 6504–6518, 2005. [Online]. Available: <http://www.opticsexpress.org/abstract.cfm?URI=OPEX-13-17-6504>
- [13] B. Potsaid, L. I. Rivera, and J. T.-Y. Wen, *Adaptive Scanning Optical Microscope (ASOM): Large Field of View and High Resolution Imaging Using a MEMS Deformable Mirror*. Bellingham, WA: SPIE, 2007, vol. 6467, 1, p. 646706. [Online]. Available: <http://link.aip.org/link/?PSI/6467/646706/1>
- [14] B. Potsaid, Y. Bellouard, and J. T. Wen, "Adaptive scanning optical microscope (ASOM) for large workspace micro-robotic applications," in *Proc. IEEE Int. Conf. Robot. Autom. (ICRA)*, New York, 2006, pp. 1024–1029.
- [15] R. E. Fischer and B. Tadij-Galeb, *Optical System Design*. New York: McGraw-Hill, 2000.
- [16] W. J. Smith, *Modern Lens Design*, 2nd ed. New York: McGraw-Hill, 2005.
- [17] G. Reimann, J. Perreault, P. Bierden, and T. Bifano, "Compact adaptive optical compensation systems using continuous silicon deformable mirrors," in *Proc. High-Resolution Wavefront Control: Methods, Devices, and Applications III*, 2001, vol. 4493, pp. 35–40.
- [18] T. Bifano, J. Perreault, P. Bierden, and C. Dimas, "Micromachined deformable mirrors for adaptive optics," in *Proc. High-Resolution Wavefront Control: Methods, Devices, and Applications IV*, 2002, vol. 4825, pp. 10–13.
- [19] Y. Zhou and T. Bifano, *Characterization of Contour Shapes Achievable With a MEMS Deformable Mirror*, S. S. Olivier, S. A. Tadigadapa, and A. K. Henning, Eds. Bellingham, WA: SPIE, 2006, vol. 6113, 1, p. 61130H. [Online]. Available: <http://link.aip.org/link/?PSI/6113/61130H/1>
- [20] J. W. Evans, K. Morzinski, S. Severson, L. Poyneer, B. Macintosh, D. Dillon, L. Reza, D. Gavel, D. Palmer, S. Olivier, and P. Bierden, *Extreme Adaptive Optics Testbed: Performance and Characterization of a 1024-MEMS Deformable Mirror*, S. S. Olivier, S. A. Tadigadapa, and A. K. Henning, Eds. Bellingham, WA: SPIE, 2006, vol. 6113, 1, p. 61130I. [Online]. Available: <http://link.aip.org/link/?PSI/6113/61130I/1>
- [21] B. C. Platt and R. Shack, "History and principles of Shack-Hartmann wavefront sensing," *J. Refractive Surgery*, vol. 17, pp. S577–S573, 2001.
- [22] D. T. Gavel, B. J. Bauman, E. W. Campbell, C. J. Carrano, and S. S. Olivier, *Practical Comparison of Phase Diversity to Interferometry in Measuring the Aberrations in an Adaptive Optics System*, R. K. Tyson and R. Q. Fugate, Eds. Bellingham, WA: SPIE, 1999, vol. 3762, 1, pp. 266–268 [Online]. Available: <http://link.aip.org/link/?PSI/3762/266/1>
- [23] M. B. Garvin, M. T. Gruneisen, R. C. Dymale, and J. R. Rotge, *Image Entropy as a Metric for Iterative Optimization of Large Aberrations*. Bellingham, WA: SPIE, 2005, vol. 5894, 1, p. 58940Y. [Online]. Available: <http://link.aip.org/link/?PSI/5894/58940Y/1>
- [24] M. Cohen, G. Cauwenberghs, and M. A. Vorontsov, "Image sharpness and beam focus VLSI sensors for adaptive optics," *IEEE Sensors J.*, vol. 2, no. 6, pp. 680–690, 2002.
- [25] R. A. Muller and A. Buffington, "Real-time correction of atmospherically degraded telescope images through image sharpening," *J. Opt. Soc. Amer. A*, vol. 64, no. 9, pp. 1200–1210, 1974.
- [26] J. E. Sulston and H. R. Horvitz, "Post-embryonic cell lineages of the nematode, *Caenorhabditis elegans*," *Dev. Biol.*, vol. 56, pp. 110–156, 1977.
- [27] J. E. Sulston, E. Schierenberg, J. G. White, and J. N. Thomson, "The embryonic cell lineage of the nematode *Caenorhabditis elegans*," *Dev. Biol.*, vol. 100, pp. 64–119, Nov. 1983.
- [28] J. G. White, E. Southgate, J. N. Thomson, and S. Brenner, "The structure of the nervous system of the nematode *Caenorhabditis elegans*," *Phil. Trans. Royal Soc. London. Series B, Biol. Sci.*, vol. 314, pp. 1–340, 1986.
- [29] C. H. Rankin, "Invertebrate learning: What can't a worm learn?," *Current Biology*, vol. 14, pp. R617–R618, Aug. 2004.
- [30] K. Strange, *C. Elegans: Methods and Applications*, K. Strange, Ed. New York: Humana Press, 2006.
- [31] M. de Bono and C. I. Bargmann, "Natural variation in a neuropeptide Y receptor homolog modifies social behavior and food response in *C. elegans*," *Cell*, vol. 94, pp. 679–689, 1998.
- [32] E. Fontaine, J. Burdick, and A. Barr, "Automated tracking of multiple *C. elegans*," in *Proc. IEEE 28th Ann. Int. Conf. Eng. Med. Biol. Soc., EMBS'06*, 2006, pp. 3716–3718.
- [33] C. J. Cronin, J. E. Mendel, S. Mukhtar, Y.-M. Kim, R. C. Stirbl, J. Bruck, and P. W. Sternberg, "An automated system for measuring parameters of nematode sinusoidal movement," *BMC Genetics*, vol. 6, pp. 1471–2156, 2005.
- [34] S. Faumont and S. R. Lockery, "The awake behaving worm: Simultaneous imaging of neuronal activity and behavior in intact animals at millimeter scale," *J. Neurophysiology*, vol. 95, pp. 1976–1981, Mar. 2006.
- [35] S. Faumont, A. C. Miller, and S. R. Lockery, "Chemosensory behavior of semi-restrained *Caenorhabditis elegans*," *J. Neurophysiology*, vol. 65, pp. 171–178, Aug. 2005.
- [36] B. Potsaid, F. P. Finger, and J. T.-Y. Wen, D. L. Farkas, R. C. Leif, and D. V. Nicolau, Eds., *Living Organism Imaging With the Adaptive Scanning Optical Microscope (ASOM)*. Bellingham, WA: SPIE, 2007, vol. 6441, 1, p. 64411D. [Online]. Available: <http://link.aip.org/link/?PSI/6441/64411D/1>
- [37] B. Potsaid, J. T. Wen, S. Barry, and A. Cable, "Commercialization of the adaptive scanning optical microscope (ASOM)," in *Proc. 6th Int. Workshop on Adaptive Optics for Industry and Medicine*, Galway, Ireland, Jun. 2007.



Benjamin Potsaid (M'05) received the Ph.D. degree in mechanical engineering from Rensselaer Polytechnic Institute, Troy, NY, in 2005, where he was a Research Scientist at the Center for Automation Technologies and Systems (CATS), Rensselaer Polytechnic Institute at the time of this research.

At CATS, he oversaw the Smart Optics Laboratory (SOL), which pursues research in novel active and adaptive optical systems and devices with biomedical, industrial, and defense applications. His research interests include optomechatronic system

design, robotics and motion control, as well as math, science, and engineering education.

Dr. Potsaid is a member of The International Society for Optical Engineers (SPIE).

Fern P. Finger received her Ph.D. degree in cell biology from Yale University, New Haven, CT, in 1998.

She performed Postdoctoral Research as a Damon Runyon Fellow at the Sloan-Kettering Institute, New York, and at the University of Wisconsin, Madison. Since 2003, she has been an Assistant Professor in the Biology Department and the Center for Biotechnology and Interdisciplinary Studies at Rensselaer Polytechnic Institute, Troy, NY. Her research concerns the roles of septins in nervous system and organ development in *C. elegans*.

Dr. Finger is a member of the American Society for Cell Biology, the Genetics Society of America, and the Society for Developmental Biology.



John T. Wen (F'01) received the B.Eng. degree from McGill University, Montreal, Canada, in 1979, the M.S. degree from the University of Illinois, Chicago, in 1981, and the Ph.D. degree from Rensselaer Polytechnic Institute, Troy, NY, in 1985, all in electrical engineering.

Since 1988, he has been at Rensselaer Polytechnic Institute where he is a Professor in the Department of Electrical, Computer, and Systems Engineering. Since July 2005, he has been the Director of the New York State Center for Automation Technologies and

Systems (CATS). His research interests lie in the areas of dynamical systems modeling, control, and planning with applications to vibration suppression, robot manipulation, biomedical systems, and network flow and power control. Dr. Wen is a Fellow of IEEE.